



## Research Paper

# Removal of chromium (VI) by a self-regenerating and metal free g-C<sub>3</sub>N<sub>4</sub>/graphene hydrogel system via the synergy of adsorption and photo-catalysis under visible light

Xing Wang<sup>a</sup>, Yinghua Liang<sup>a,\*</sup>, Weijia An<sup>a</sup>, Jinshan Hu<sup>a</sup>, Yongfa Zhu<sup>b</sup>, Wenquan Cui<sup>a,\*</sup><sup>a</sup> College of Chemical Engineering, Hebei Key Laboratory for Environment Photocatalytic and Electrocatalytic Materials, North China University of Science and Technology, Tangshan, 063210, PR China<sup>b</sup> Department of Chemistry, Tsinghua University, Beijing, 100084, PR China

## ARTICLE INFO

## Article history:

Received 23 April 2017

Received in revised form 15 June 2017

Accepted 3 July 2017

Available online 12 July 2017

## Keywords:

Photo-catalysis

Adsorption

Graphene hydrogel

Cr (VI) removal

Metal free

## ABSTRACT

We propose g-C<sub>3</sub>N<sub>4</sub> nano-sheets and a graphene three-dimensional (3D) gel system composed of two metal free nano-sheets of g-C<sub>3</sub>N<sub>4</sub> and graphene via the stacking effect of two-dimensional (2D) nano-sheets and the π-π conjugated at low temperature. This material has self-regeneration and containing only C and N, which confirms the ability to efficiently remove chromium (VI) (Cr(VI)) via the synergistic effect of adsorption and photo-catalysis. The graphene sheets offer surface adsorption in the composite, which can lead to the adsorption of Cr (VI) with high adsorption capacity and fast speed. The g-C<sub>3</sub>N<sub>4</sub> nano-sheets have high photocatalytic activity *in situ* for composite to absorb the high toxicity of Cr (VI). This was rapidly reduced to Cr (III). The adsorption and photocatalytic degradation synergized to achieve self-regeneration. The results showed that 80% Cr (VI) (30 mg/L) can be adsorbed by composite in 30 min, and the removal of Cr (VI) reached 100% in 120 min under visible light irradiation via adsorption and photo-catalysis. The low concentrations (2 mg/L) of Cr (VI) can be achieved via a degradation rate of almost 100% that was maintained for more than 26 h. At the same time, there was a large quantity of hydrogel in the pore space network and micron level structure in the composite. This offers 99% recycling and reuse via a stainless steel filter (pore size 38 μm) without the need to rely on a complex separation system. This solves the difficult problems of powder catalyst recovery.

© 2017 Elsevier B.V. All rights reserved.

## 1. Introduction

Heavy metal chromium is widely used in the fields of steel, pigment, electroplating, etc. but it has strong toxicity. Cr (VI) in particular can cause serious pollution when discharged into the water [1]. Once the concentration of chromium in drinking water exceeds 0.1 mg/L, it can cause abdominal pain, dizziness, diarrhea, and other symptoms even leading to a variety of diseases such as cancer and fetal malformations [2]. The World Health Organization (WHO) stipulates that Cr (VI) in drinking water shall not exceed 0.003 mg/L [3], and the Environmental Protection Agency (EPA) recommends that Cr (VI) concentrations in water should be less than 0.005 mg/L [4]. Therefore, it has very important scientific and practical value in the removal of Cr (VI) from water.

Traditional treatment methods use adsorption to deal with the low concentration of chromium ions in water [5]. However, this approach has some shortcomings such as low purification efficiency, easy saturation, regeneration difficulties, and high cost. Activated carbon (AC) adsorption materials are commonly used [6–8], and porous materials with a high surface area offer high adsorption performance. These are used for the adsorption of heavy metals for pore-adsorption, and diffusion adsorption effects lead to slow speeds, high cost, and slow regeneration.

The 2D layered graphene has a high specific surface area and high surface adsorption. It has important application value in heavy metal adsorption and removal [9]. The 3D gels composed of two layers of thin films have a large pore structure and an interconnection network. The pore structure of the gel is on the micron regime. Therefore, the regeneration and the separation of the gel is simple, which is convenient for recycling. The 3D gels have a high specific surface area and cross layer accumulation through pores [10], large adsorption capacity, and easy regeneration. Thus, it has broad util-

\* Corresponding authors.

E-mail addresses: liangyh@ncst.edu.cn (Y. Liang), wkcui@163.com (W. Cui).

ity in water purification (adsorption of heavy metals [11], organic matter [12], gas [13], offshore oil [14], etc.)

In addition, the highly toxic Cr (VI) in water was reduced to chromium (III) via a photocatalytic reduction [15]. This offers environmental friendliness and high efficiency. Photocatalytic technology has broad applications in environment management. More recently, researchers have been actively looking for high quantum yield photo-catalysts, and related work has been reported [16–20]. Most of the photo-catalysts are expensive metal-based powders [21] with UV light that cannot be completely separated from the water. Thus results in new metal pollutants in the water. Research on the free-metal photocatalytic materials with a high utilization rate of solar energy and improved recycling ability of materials will greatly promote the development of photocatalytic reduction of Cr (VI).

Polymer g-C<sub>3</sub>N<sub>4</sub> is a free metal semiconductor material containing only C and N with visible light response ( $E_g = 2.7$  eV), environmental friendliness, and low toxicity. Owing to its advantages of low cost and high abundance, it has been applied to process various pollutants in the water [18–20]. Liu et al. [22] used it to reduce Cr (VI) via a metal matrix composite g-C<sub>3</sub>N<sub>4</sub>, and the effective degradation was achieved for Cr (VI) (30 mg/L) containing wastewater. Various forms of g-C<sub>3</sub>N<sub>4</sub> have been reported [23–25] including 2D nano-sheets with more active sites and low hardness to reduce the transverse dimension. The structural anisotropy reduces the migration distance of charge in a plane to improve the catalytic capacity [26,27]. However, there are some limitations: the g-C<sub>3</sub>N<sub>4</sub> nano-sheets must be gathered when used in water treatment, and the impact of its surface area led to a reduction in adsorption capacity. Also, working on the nano-scale materials make it difficult to recycle, resulting in a waste of resources.

In recent years, multiple studies have shown that the combination of adsorbent and photo-catalyst [28–30] coupled with adsorption and photo-catalysis of these two methods can improve remediation. Here, the catalyst is supported on 3D adsorption material. Previous reports by Zhang et al. [31] showed that the photocatalytic materials on the nano-scale were immobilized on a silica gel, and the adsorption and catalysis were synergistic. This improves the performance of the material. However, the conductivity of silicon is weak, and the transfer rate of the photo-generated charge cannot be enhanced. In our previous work [32], the TiO<sub>2</sub> nanoparticles were combined with a graphene hydrogel to form a three-dimensional network structure of hydrogel system. High conductivity graphene can separate the photo-generated charge of the TiO<sub>2</sub> nanoparticles, and the photocatalytic activity can be maintained at a high level. Graphene hydrogel can quickly adsorb and enrich chromium ions. Meanwhile, the TiO<sub>2</sub> nanoparticles offer *in situ* catalytic degradation, and the synergistic effect is realized for the removal of heavy metal ion adsorption and photocatalysis. This improves the removal rate of Cr (VI) under ultraviolet light. The structure of the micron is conducive to the rapid separation of composites.

Here, we further synthesized the g-C<sub>3</sub>N<sub>4</sub> nano-sheets/rGH (g-C<sub>3</sub>N<sub>4</sub>/rGH) to form a new 3D hydrogel with free-metal material and visible light response and successfully used it to remove Cr (VI). The porous network structure of the hydrogel has high adsorption capacity, and the g-C<sub>3</sub>N<sub>4</sub> nano-sheets can adsorb Cr (VI) reduced to Cr (III) *in situ* under visible light. The synergistic effects of adsorption and photocatalysis are realized. The g-C<sub>3</sub>N<sub>4</sub> nano-sheets and graphene nano-sheets were cross-stacked to effectively prevent aggregation of the catalyst and avoid increasing the density of the hydrogel, damaging the structure, etc. The 3D network structure of the micron size can avoid the tedious operation of powder material when it is separated. The filtering operation method offers normal pressure operation, high efficiency, low cost, etc.

## 2. Experimental methods

### 2.1. Preparation of the g-C<sub>3</sub>N<sub>4</sub>/rGH hybrid hydrogels

Graphite powder (325 mesh) was purchased from Chemical Reagent Center of Beijing. Dicyandiamide was purchased from Yongda Chemical Reagent Corp. All other reagents used in this research were analytically pure and used without further purification.

The g-C<sub>3</sub>N<sub>4</sub> nano-sheet was prepared via pyrolysis of cyanurotriamide in air [20]: 5 g of cyanurotriamide was placed into an alumina crucible with a cover and heated from 30 °C to 550 °C with a heating rate of 1 °C/min in a muffle furnace and maintained at this temperature for 4 h. The yellow powder is bulk g-C<sub>3</sub>N<sub>4</sub>. The g-C<sub>3</sub>N<sub>4</sub> nano-sheet was prepared by calcining the bulk g-C<sub>3</sub>N<sub>4</sub> under the same conditions again.

Graphite oxide (GO) was synthesized by a method modified from the Hummers method [33]: 3 g graphite (325 mesh) was added to 70 ml of H<sub>2</sub>SO<sub>4</sub> (98 wt%) in an ice bath and stirred for 10 min followed by 1.5 g of NaNO<sub>3</sub> and 9 g of KMnO<sub>4</sub>. The mixture was cooled to below 20 °C and stirred for 2.5 h. This was then increased to 35 °C and held for 3.5 h. Next, 150 ml of deionized water was added to the solution and heated to 95 °C. This was stirred for 1.5 h. Next, we gradually added 300 ml of deionized water and 20 ml of H<sub>2</sub>O<sub>2</sub> (30 wt%). The reaction products were washed and centrifuged with HCl (10 wt%) and dialyzed against water for 7 days to obtain graphene oxide (GO).

The synthesis of rGH used the literature [34] with minor modifications. The g-C<sub>3</sub>N<sub>4</sub> nano-sheets were added to 30 ml GO (2 mg/L), and the solution was mixed with ultrasonic treatment for 30 min. The g-C<sub>3</sub>N<sub>4</sub> nano-sheets was added as a mass ratio of X (X = 30%, 50%, 70%, 90%). Then, 6 g sodium ascorbate was added with stirring for 30 min, and then the temperature was increased to 95 °C and for 60 min. Then, a series of X g-C<sub>3</sub>N<sub>4</sub>/rGH hydrogels were obtained. Similar experiments were carried out to synthesize the bulk 90% g-C<sub>3</sub>N<sub>4</sub>/rGH and 90% TiO<sub>2</sub>/rGH. In addition to replacing the bulk g-C<sub>3</sub>N<sub>4</sub> and the TiO<sub>2</sub> with the g-C<sub>3</sub>N<sub>4</sub> nano-sheets, other experimental conditions remain unchanged in the accompanying process.

### 2.2. Characterization

The crystal structure and phase state of the samples were determined by X-ray diffractometry (XRD) using a Rigaku D/MAX2500 PC diffractometer with Cu K $\alpha$  radiation at an operating voltage of 40 kV, an operating current of 100 mA, and a scanning range from 5 to 80°. The morphology and size of the samples were imaged with a scanning electron microscopy (SEM) using a Hitachi S-4800 SEM microscope and with transmission electron microscopy (TEM) using a JEOL JEM-2010 TEM microscope and electron beam acceleration voltage of 100 kV. Raman spectra were recorded on a microscopic confocal Raman spectrometer (Thermo Electron DXR) with an excitation wavelength at 524 nm and 785 nm. The Fourier transform infrared (FT-IR) spectra of the samples were recorded on a Thermo Nicolet Avatar 370 spectrometer. The chemical states of the photo-catalysts were analyzed via X-ray photoelectron spectroscopy (XPS) using an XSAM800 apparatus. Photoluminescence (PL) spectra were recorded on a Hitachi F-7000 spectrometer with an excitation wavelength at 320 nm. UV-vis diffuse reflectance spectra were recorded on a UV-vis spectrometer (Puxi, UV1901) with BaSO<sub>4</sub> as the reference sample. The specific surface area ( $S_{BET}$ ) of the sample was characterized by nitrogen adsorption at 77 K with a Micromeritics 3020 instrument.

### 2.3. Synergy of adsorption and photo-catalysis in removing Cr(VI)

#### 2.3.1. Static reaction: photo-catalysis and adsorption in removing Cr(VI)

The adsorption and photocatalytic experiments were carried out in the photochemical reaction instrument (XPA-7). A visible light source was obtained via a 400 W metal halide lamp with a 420 nm cutoff filter. The  $K_2Cr_2O_7$  was dissolved in deionized water to form a Cr (VI) solution as the degradation target. The equivalent mass is obtained by referring to 90% g-C<sub>3</sub>N<sub>4</sub>/rGH.

First, we evaluated the adsorption performance in the dark. The 30 ml of Cr (VI) (30 mg/ml) was added to 50 ml of the reaction tube with a plug. This was then treated with 30 mg g-C<sub>3</sub>N<sub>4</sub>/rGH composites and maintained at  $25 \pm 2^\circ\text{C}$  with stirring for 60 min to achieve adsorption and desorption equilibrium in the dark. Next, we performed photocatalytic reduction of Cr (VI) under visible light. The degradation reaction time was 120 min during which 1.5 ml samples were taken every 10 min. The composites were then separated via a high-speed centrifuge to remove the catalyst in the sample, and then the concentration of Cr (VI) in the supernatant was determined.

Under the same conditions, g-C<sub>3</sub>N<sub>4</sub> nano-sheets, rGH, and 90% g-C<sub>3</sub>N<sub>4</sub>/rGH were used to degrade the target pollutant Cr (VI) (5 mg/L) 10 times to evaluate the catalytic stability and recyclability. Here, 30 ml Cr (VI) (30 mg/L) was added to a 50 ml reaction tube with a stopper followed by 30 mg 90% g-C<sub>3</sub>N<sub>4</sub>/rGH catalyst at  $25 \pm 2^\circ\text{C}$ . The light was used for the experiment of adsorption and photocatalytic reduction of Cr (VI). The total time is 120 min. After each experiment, we determined the final concentration of Cr (VI), filtered the samples by using 38  $\mu\text{m}$  stainless steel filter, and used the deionized water to wash the samples, without needing elution treatment.

#### 2.3.2. Continues flow reaction: synergy of photo-catalysis and adsorption in removing Cr(VI)

The experiment was conducted in a self-made reactor. The 100 mg of a hydrogel was added to a polyfluorotetraethylene groove ( $40\text{ mm} \times 20\text{ mm} \times 2\text{ mm}$ ), and the quartz glass was sealed. The inlet and outlet ports were on the sides. A peristaltic pump (Baoding Constant flow pump Co., Ltd. YZ1515) was used to control the solution flow rate. A visible light source was obtained with a 500 W Xe lamp (CHF-XW-500) with a 420 nm cutoff filter, which is 10 cm away from the reactor. We used 0.1 g of rGH and 90% g-C<sub>3</sub>N<sub>4</sub>/rGH at 2 mg/L Cr (VI) and a flow rate of 0.16 ml/min. The 1.5 ml samples were taken every 60 min.

The concentration of total Cr was determined via an inductively coupled plasma (ICP) direct reading spectrometer. The concentration of Cr(VI) was determined by the diphenyl hydrazine method, and the concentration of Cr(III) was calculated by subtracting the Cr(VI) concentration from the total Cr concentration.

## 3. Results and discussion

### 3.1. The 3D network gel structure and phase state

XRD was used to investigate the structures of GO, rGH, g-C<sub>3</sub>N<sub>4</sub> nano-sheets, and X g-C<sub>3</sub>N<sub>4</sub>/rGH (X = 30%, 50%, 70%, 90%) (Fig. 1). The GO spectrum and rGH spectrum are compared, which illustrates the change in diffraction peaks in the reduction process for GO. In the GO spectrum, the 001 diffraction peak of  $2\theta=12.1^\circ$ , and the corresponding interlayer space is about 0.76 nm. Due to the presence of a large number of oxygen-containing groups such as hydroxyl, carbonyl, epoxy, etc. [33], the graphite is successfully stripped into the GO thin film. The GO was reduced to rGH by sodium ascorbate, and the rGH diffraction peak at  $25.1^\circ$  indicates that a large number of oxygen-containing functional groups were removed. The

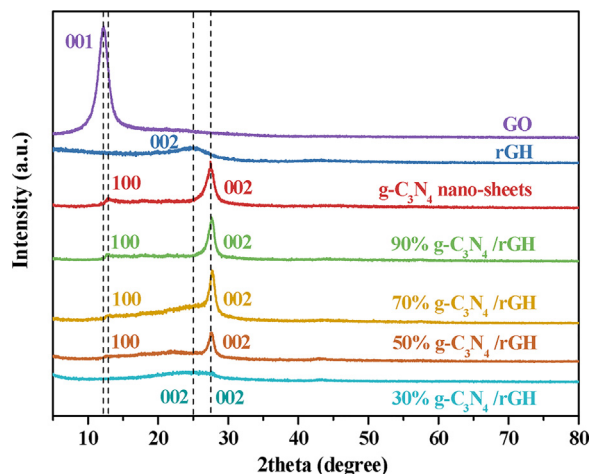


**Fig. 1.** XRD spectra of GO, rGH, g-C<sub>3</sub>N<sub>4</sub> nano-sheets, and X g-C<sub>3</sub>N<sub>4</sub>/rGH (X = 30%, 50%, 70%, 90%).

corresponding interlayer space is about 0.36 nm. The intensity of the peak decreases and becomes wider, which is attributed to the transition from graphite to graphite sheets [35].

The two peaks at  $12.8^\circ$  (100) and  $27.6^\circ$  (002) of g-C<sub>3</sub>N<sub>4</sub> nano-sheets correspond to the in-plane ordering of the tri-s-triazine units and graphitic structure [36]. The diffraction peak in the same position for X g-C<sub>3</sub>N<sub>4</sub>/rGH (X = 70%, 90%) hybrid hydrogels and g-C<sub>3</sub>N<sub>4</sub> nano-sheets are due to the high content of g-C<sub>3</sub>N<sub>4</sub> nano-sheets in the composite. This showed a slight characteristic peak belonging to rGH. The diffraction peaks (002) of rGH were not obvious due to the overlap with g-C<sub>3</sub>N<sub>4</sub> nano-sheets. The X g-C<sub>3</sub>N<sub>4</sub>/rGH (X = 30%, 50%) hybrid hydrogels have a weak peak at  $25.1^\circ$  of rGH. This might be because rGH has high dispersion and larger size than g-C<sub>3</sub>N<sub>4</sub> nano-sheets. Thus, they cannot be completely shielded.

The morphology and element of the samples were imaged with SEM, TEM, HR-TEM, TEM mapping and TEM-EDS (Fig. 2). The composite's 3D mesh skeleton is clearly seen in Fig. 2a. The gel structure is not affected by the presence of g-C<sub>3</sub>N<sub>4</sub> nano-sheets, and the pore diameter is about a few microns, and the pores are very dispersed. TEM and HR-TEM images (Fig. 2b and c) show that the g-C<sub>3</sub>N<sub>4</sub> nano-sheets are uniformly dispersed on thin films of the rGH, and there is no agglomeration, which can be seen in the rGH films with multiple folds that are different from those of the g-C<sub>3</sub>N<sub>4</sub> sheets. The g-C<sub>3</sub>N<sub>4</sub> sheets prevent further crimping and collapse of the rGH films. TEM mapping and TEM-EDS (Fig. 2d, and e) analysis of the composite shows C, N and O. Both have nearly transparent lamellae, and all atom concentration is lower. Here, the C and O are from g-C<sub>3</sub>N<sub>4</sub> nano-sheets, rGH, and Carbon supported membrane. The Cu elements are from the copper mesh. The N elements are from g-C<sub>3</sub>N<sub>4</sub> nano-sheets. It shows that the high content of g-C<sub>3</sub>N<sub>4</sub> nano-sheets is uniformly dispersed in the 3D gel system.

The FT-IR spectra of the samples are shown in Fig. 3. Three peaks at  $3435\text{ cm}^{-1}$ ,  $1622\text{ cm}^{-1}$ , and  $1063\text{ cm}^{-1}$  of rGH. This corresponds to the stretching peak of O—H, C=C framework of graphite aromatic rings and the stretching peak of C—O [35]. The bands at  $3200\text{ cm}^{-1}$ ,  $1500\text{ cm}^{-1}$ , and  $806\text{ cm}^{-1}$  for g-C<sub>3</sub>N<sub>4</sub> sheets can be attributed to the NH and OH stretching of vibrational peaks in the incomplete poly-condensation of product edge, the stretching of aromatic CN heterocycle, and the breathing of the triazine unit [36]. The characteristic peaks of 90% g-C<sub>3</sub>N<sub>4</sub>/rGH are similar to those of g-C<sub>3</sub>N<sub>4</sub> nano-sheets because of the high content of g-C<sub>3</sub>N<sub>4</sub> nano-sheets. However, the characteristic peaks of rGH are not obvious because of the overlap and low intensity. There were no new characteristic peaks in the composite, which indicated that the hybridization did not produce other unique molecular bonds.

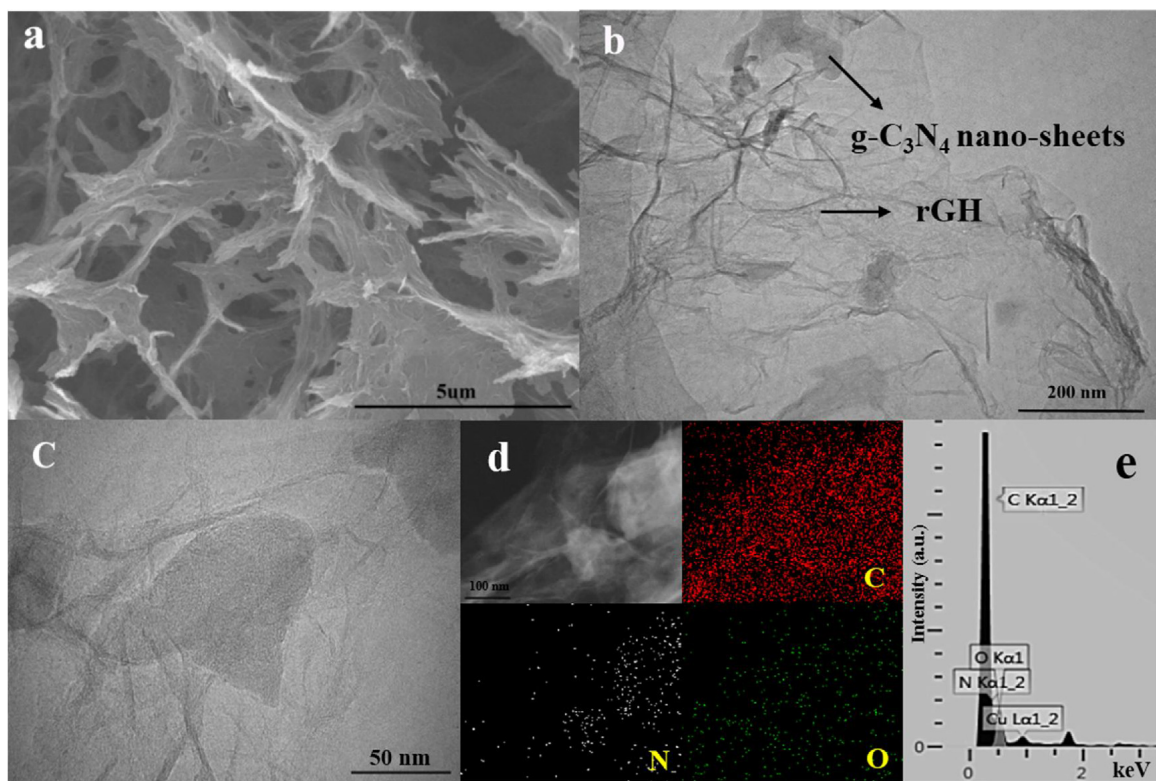


**Fig. 2.** (a) SEM image, (b) TEM image, (c) HR-TEM analysis, (d) TEM mapping, and (e) TEM-EDS image of 90% g-C<sub>3</sub>N<sub>4</sub>/rGH.

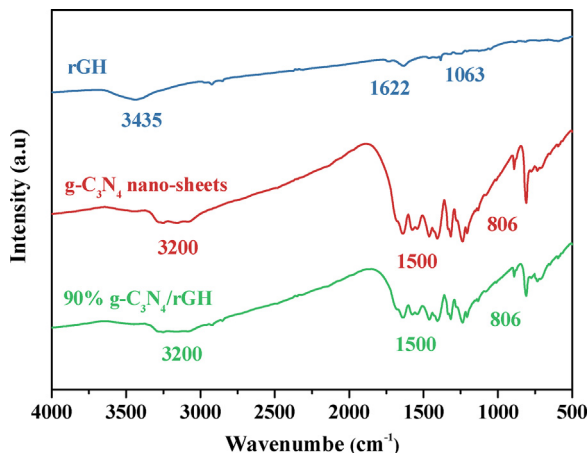


**Fig. 3.** FT-IR spectra of rGH, g-C<sub>3</sub>N<sub>4</sub> nano-sheets, and 90% g-C<sub>3</sub>N<sub>4</sub>/rGH.

The atomic structure and electronic properties of materials were further analyzed by Raman. The GO and the rGH have two sharp and strong characteristic peaks at 1350 cm<sup>-1</sup> and 1580 cm<sup>-1</sup> (Fig. 4). These are the D peak and G peak. The D peak represents the defect of the graphene edge and its amorphous structure due to some oxygen-containing functional groups. The G peak represents the ordered bond structure of sp<sup>2</sup> [37]. Versus GO, the values of I<sub>D</sub>/I<sub>G</sub> increased significantly indicating that there are some defects in the prepared rGH. Some oxygen-containing functional groups have not been reduced, which is consistent with the analysis of FT-IR. The characteristic peaks were at 472 cm<sup>-1</sup>, 707 cm<sup>-1</sup>, 769 cm<sup>-1</sup>, 979 cm<sup>-1</sup>, and 1311 cm<sup>-1</sup> in g-C<sub>3</sub>N<sub>4</sub> nano-sheets, respectively. These are consistent with values reported previously [38]. The peaks of 90% g-C<sub>3</sub>N<sub>4</sub>/rGH appeared at 452 cm<sup>-1</sup>, 668 cm<sup>-1</sup>, 730 cm<sup>-1</sup>, and 1156 cm<sup>-1</sup>, and all of these belonged to the characteristic peaks of g-C<sub>3</sub>N<sub>4</sub> nano-sheets. The low content of rGH did not

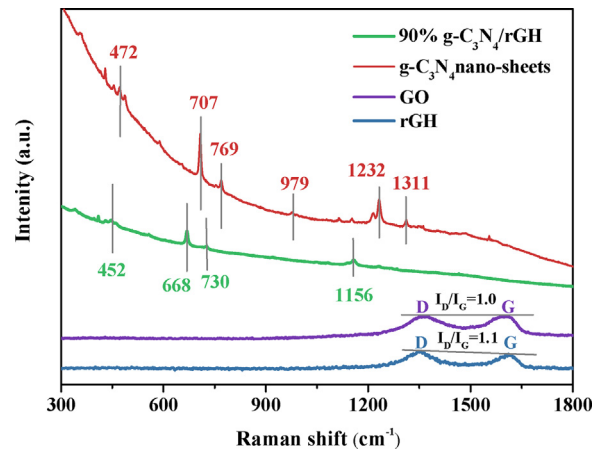


**Fig. 4.** Raman spectra of GO, rGH, g-C<sub>3</sub>N<sub>4</sub> nano-sheets, and 90% g-C<sub>3</sub>N<sub>4</sub>/rGH.

appear in the composite spectra. All peaks are red shifted, and some peaks disappear. This may be masked by the low peak intensity and the π-π conjugated interaction between g-C<sub>3</sub>N<sub>4</sub> nano-sheets and rGH.

XPS was used to analyze the elemental composition and bonding of 90% g-C<sub>3</sub>N<sub>4</sub>/rGH. Fig. 5a shows that there are three elements of C, N and O in the composite. In Fig. 5b, the C 1 s spectra was divided into three characteristic peaks of 284.8 eV, 286.5 eV, and 288.8 eV, respectively. These correspond to the sp<sup>2</sup> of C–C, C–O, and N=C=N in the molecular structure of g-C<sub>3</sub>N<sub>4</sub> nano-sheets [38,39]. In the N 1 s spectra (Fig. 5c), three characteristic peaks can be separated including 399.4 eV, 400.9 eV, and 405.9 eV, respectively, from the sp<sup>2</sup> structure of N(C=N–C), N-(C)<sub>3</sub>, and –NH<sub>2</sub> or =NH functional groups [40]. The O 1 s spectra (Fig. 5d) shows the presence of –OH in the composite.

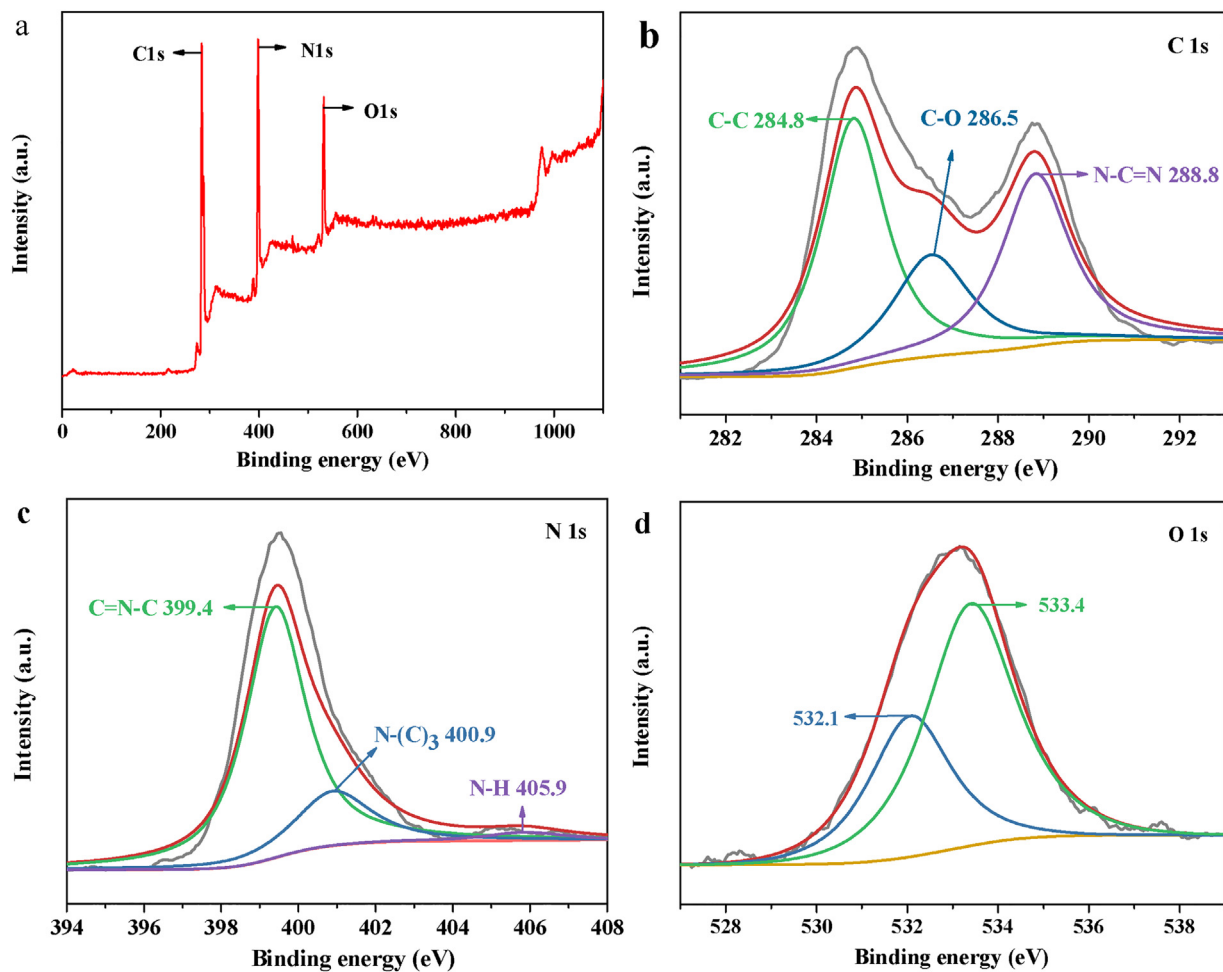


**Fig. 5.** (a) Survey XPS spectra for 90%  $\text{g-C}_3\text{N}_4/\text{rGH}$ , (b) C 1s, (c) N 1s, and (d) O 1s for 90%  $\text{g-C}_3\text{N}_4/\text{rGH}$ .

### 3.2. The high utilization efficiency of visible light

The UV-vis diffuse reflectance of the samples is shown in Fig. 6a. The rGH enables the hydrogels to absorb at all wavelengths. The calculated band gap is shown (Fig. 6b) in which the band gap of  $\text{g-C}_3\text{N}_4$  nano-sheets ( $E_g = 2.71 \text{ eV}$ ) is lower than that of bulk  $\text{g-C}_3\text{N}_4$  ( $E_g = 2.75 \text{ eV}$ ). Therefore, the composites still absorb in the visible region. The results showed that the  $\text{g-C}_3\text{N}_4/\text{rGH}$  hydrogel could effectively increase the absorption range of visible light and improve the absorption and utilization of visible light. The PL spectrum (Fig. 6c) of 90%  $\text{g-C}_3\text{N}_4/\text{rGH}$  reveals a much lower intensity than that of  $\text{g-C}_3\text{N}_4$  nano-sheets, but the emission wavelength of  $\text{g-C}_3\text{N}_4$  nano-sheets and 90%  $\text{g-C}_3\text{N}_4/\text{rGH}$  is similar to that of the photoluminescence spectra. There is no obvious displacement in the spectra. This indicates that the radiative recombination of photo-generated electron-hole pairs is inhibited [41,42]. Fig. 6d illustrates that the photocurrent response of  $\text{g-C}_3\text{N}_4$  nano-sheets increased significantly, but the photo-generated charge resulted in rapid recombination of the phenomenon. This does not appear in the 90%  $\text{g-C}_3\text{N}_4/\text{rGH}$ , and the photocurrent response is greatly improved.

### 3.3. The hybrid hydrogels to remove Cr(VI) efficiently via the synergistic effect of adsorption and photo-catalysis

In order to illustrate the pore structure and surface area of the material, we carried out  $\text{N}_2$  adsorption-desorption test on 90%  $\text{g-C}_3\text{N}_4/\text{rGH}$  and rGH. Fig. 7a BJH  $\text{N}_2$  adsorption-desorption curves

**Table 1**  
Adsorption kinetics parameters of rGH and 90%  $\text{g-C}_3\text{N}_4/\text{rGH}$ .

Samples	$S_{\text{BET}}(\text{m}^2\text{g}^{-1})$	Pore volume ( $\text{cm}^3\text{g}^{-1}$ )	Mostly pore Diameter(nm)
rGH	217.8389	1.1867	3.94
g-C <sub>3</sub> N <sub>4</sub> /rGH	302.6557	1.4855	3.90

show that there is a slight adsorption leap at the low specific pressure, which indicates the possibility of the existence of microporous structures. There is a significant hysteresis loop and a sudden jump in  $P/P_0 = 0.5-1.0$ , which shows the characteristics of the mesoporous material, indicating that there are interconnected channels within the samples.  $\text{N}_2$  adsorption-desorption isotherms of two samples are similar and all of them are type IV isotherms of the IUPAC. Fig. 7b (the inset) shows that the pore size of the samples is mostly 3.9 nm, and there are some mesoporous and macroporous. According to the convention in IUPAC, the shape of the hysteresis loop indicates that the holes are slits and conical shapes. Fig. 7c shows that the volume of the composites increased after freeze-drying compared to rGH. The result is the same as in Table 1, which will be beneficial to improve the adsorption performance. After freeze-drying, 90%  $\text{g-C}_3\text{N}_4/\text{rGH}$  still offers a better morphology than 90%  $\text{TiO}_2/\text{rGH}$ . It also showed that  $\text{g-C}_3\text{N}_4$  nano-sheets did not affect the gelation process of rGH.

The stainless-steel mesh was used to filter and separate the materials. Table 2 shows test data of different pore diameters for the different materials. When the  $\text{TiO}_2$ , 90%  $\text{TiO}_2/\text{rGH}$ ,  $\text{g-C}_3\text{N}_4$  nano-

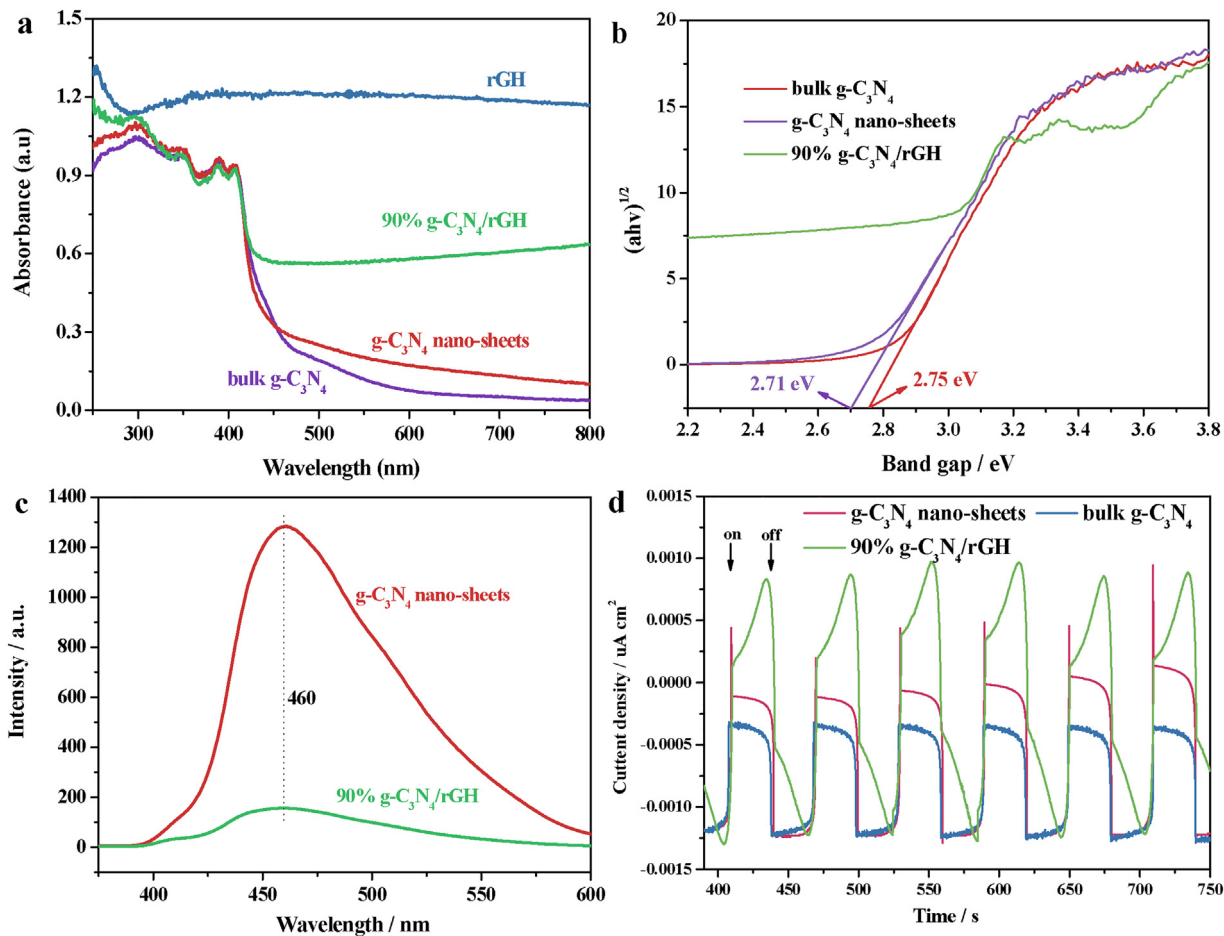


**Fig. 6.** (a) UV-vis diffuse reflectance of bulk  $\text{g-C}_3\text{N}_4$ , rGH,  $\text{g-C}_3\text{N}_4$  nano-sheets, and 90%  $\text{g-C}_3\text{N}_4/\text{rGH}$ , (b) plots of  $(\alpha h\nu)^{1/2}$  versus photon energy ( $h\nu$ ) of bulk  $\text{g-C}_3\text{N}_4$ ,  $\text{g-C}_3\text{N}_4$  nano-sheets, and 90%  $\text{g-C}_3\text{N}_4/\text{rGH}$ , (c) photoluminescence spectra of  $\text{g-C}_3\text{N}_4$  nano-sheets, and 90%  $\text{g-C}_3\text{N}_4/\text{rGH}$ , and (d) photocurrent-time curves of bulk  $\text{g-C}_3\text{N}_4$ ,  $\text{g-C}_3\text{N}_4$  nano-sheets, and 90%  $\text{g-C}_3\text{N}_4/\text{rGH}$  under visible light ( $> 420 \text{ nm}$ ) irradiation with 30 s light on/off cycles.

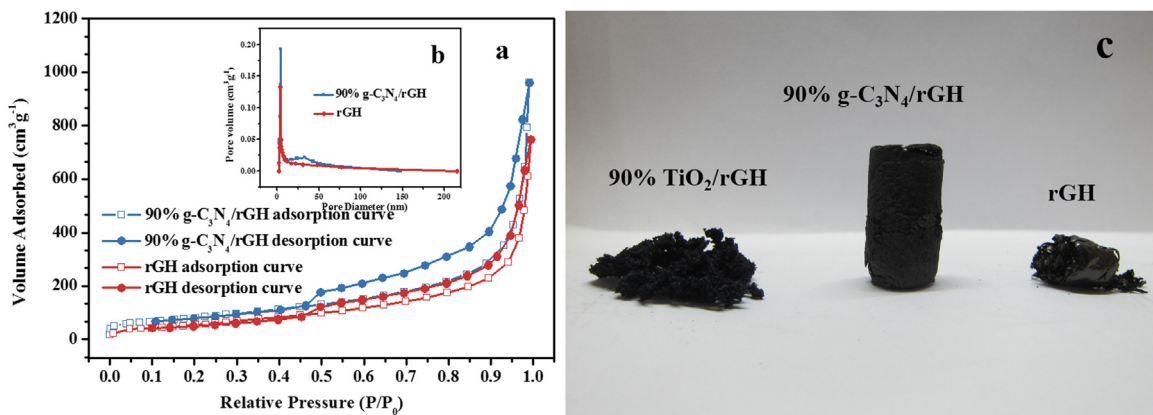


**Fig. 7.** (a) BJH nitrogen adsorption-desorption isotherms, (b) the corresponding pore size distribution plots (inset) of 90%  $\text{g-C}_3\text{N}_4/\text{rGH}$  and rGH, and (c) Hybrid hydrogels in real images.

**Table 2**  
The interception rate of different pore sizes for different materials.

Strainer (pore diameter)	TiO <sub>2</sub>	90% TiO <sub>2</sub> /rGH	$\text{g-C}_3\text{N}_4$ nano-sheets	90% $\text{g-C}_3\text{N}_4/\text{rGH}$
38 um	0%	74%	5%	95%
75 um	0%	55%	0%	93%
150 um	0%	11%	0%	85%
180 um	0%	0%	0%	76%
380 um	0%	0%	0%	40%

sheets and 90%  $\text{g-C}_3\text{N}_4/\text{rGH}$  were filtered (38  $\mu\text{m}$ ), the interception rate of  $\text{TiO}_2$  and  $\text{g-C}_3\text{N}_4$  nano-sheets were only 0% and 5%, but the hybrid hydrogels were improved (90%  $\text{TiO}_2/\text{rGH}$  was 74%, and 90%  $\text{g-C}_3\text{N}_4/\text{rGH}$  was 99%). We concluded that the hybrid hydrogels are the easiest to separate via a stainless-steel filter. It also shows that 90%  $\text{g-C}_3\text{N}_4/\text{rGH}$  have better mechanical strength than 90%  $\text{TiO}_2/\text{rGH}$ , this is consistent with the conclusion of Fig. 7c. Its good mechanical strength reduces the recovery requirements. The only need is the pore diameter of the filter screen. The recovery

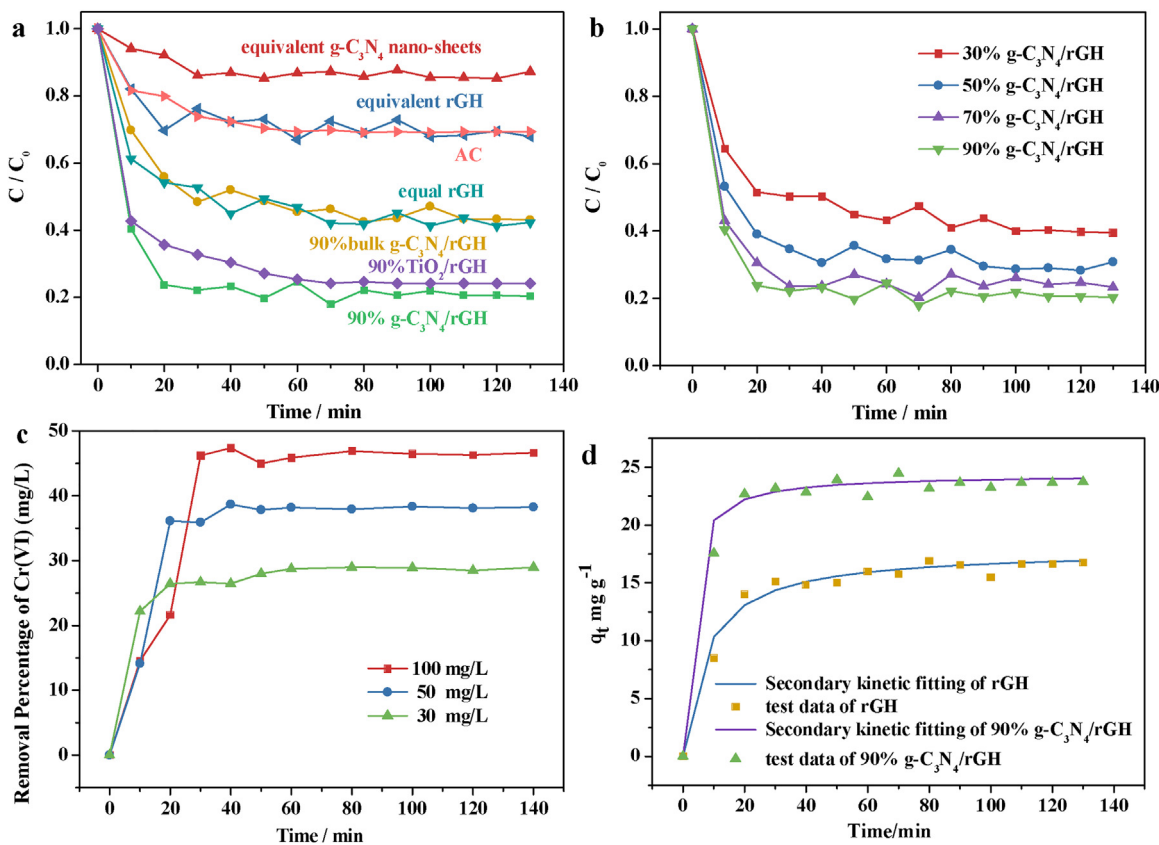


**Fig. 8.** (a) Cr(VI) adsorption capacity of different composite materials. (b) Cr(VI) adsorption capacity of a series of hybrid hydrogels. (c) The adsorption capacity test of 90%  $\text{g-C}_3\text{N}_4/\text{rGH}$ . (d) Pseudo-second order model of rGH and 90%  $\text{g-C}_3\text{N}_4/\text{rGH}$ .

rate can reach more than 99% without additional pressure. This reduces energy consumption and eliminates the cost of recycling and regeneration.

The Cr(VI) adsorption capacity of different composite materials can be observed by Fig. 8a. The results show that 80% Cr (VI) (30 mg/L) can be adsorbed by 90%  $\text{g-C}_3\text{N}_4/\text{rGH}$  in 30 min. The weak adsorption of  $\text{g-C}_3\text{N}_4$  nano-sheets is derived from the voids or flaws on the surface of the tri-s-triazine units [43]. The adsorption capacity of rGH is twice as large as that of AC because of the different modes of pore-adsorption and surface-adsorption. The differences in adsorption capacity of bulk 90%  $\text{g-C}_3\text{N}_4/\text{rGH}$ , 90%  $\text{TiO}_2/\text{rGH}$ , and 90%  $\text{g-C}_3\text{N}_4/\text{rGH}$  derived from a nano size in water can be highly dispersed. This affects the  $\pi-\pi$  conjugated synergistic effect of graphite layers. This prevented the flexible graphene thin films from collapsing and aggregating during 3D gelation. We concluded that in the dark, the  $\text{g-C}_3\text{N}_4$  nano-sheets can promote the adsorption capacity of graphene, and this causes the volume of the hydrogel to increase and the surface area to become larger. The adsorption properties of all composites improved in Fig. 8b. The best adsorption was 90%  $\text{g-C}_3\text{N}_4/\text{rGH}$  hybrid hydrogels. Moreover, the adsorption capacities of 70%  $\text{g-C}_3\text{N}_4/\text{rGH}$  and the like were approximately the same as that of 90%  $\text{g-C}_3\text{N}_4/\text{rGH}$ . The adsorption of different concentrations of pollutants (Fig. 8c) can be observed for 100 mg/L, 50 mg/L, and 30 mg/L Cr (VI) solution. The equilibrium of the adsorption value reached 49.73 mg/g, 40.63 mg/g, and 28.24 mg/g, individually. The rGH has a well-developed pore structure and a large specific surface area, and the hydrogels have a high adsorption capacity. The calculated data of  $q_e$  are consistent with the experimental results (Fig. 8d and Table 3). The coefficient of determination  $R^2$  of the pseudo-second order model is as high

as 0.999. This is much higher than the pseudo-first order kinetic model ( $R^2 = 0.844$ ) indicating that 90%  $\text{g-C}_3\text{N}_4/\text{rGH}$  and rGH hydrogel adsorb Cr (VI) is more suitable for a pseudo-second kinetic model.

Adsorption and photo-catalysis capacity of different composite materials for removing Cr(VI) (Fig. 9a). After 60 min of adsorption in the dark, there is an equilibrium state. Then, the photocatalytic reduction reaction proceeds under visible light. The activity of 90%  $\text{g-C}_3\text{N}_4/\text{rGH}$  is improved after illumination, which shows that it can remove Cr (VI) via reduction. Compared with the data of rGH, we found that the composites under visible light, can still maintain the catalytic activity, and the catalytic rate is slightly larger than that of  $\text{g-C}_3\text{N}_4$  nano-sheets alone. This indicates that the rGH is beneficial to transfer charge and reduce recombination of photo-generated electron-hole pairs. This result is consistent with the photocurrent-time curve analysis.

The  $\text{TiO}_2/\text{rGH}$  cannot absorb visible light in the adsorption equilibrium, and it cannot continue to degrade Cr (VI). The  $\text{g-C}_3\text{N}_4$  nano-sheets have more active sites than bulk  $\text{g-C}_3\text{N}_4$ . After adsorption equilibrium, 90%  $\text{g-C}_3\text{N}_4/\text{rGH}$  still have high efficiency to degrade low concentrations of Cr (VI). In addition, the  $\text{g-C}_3\text{N}_4$  nano-sheets of the hydrogel have a rich active site, while the  $\text{g-C}_3\text{N}_4$  nano-sheets promoted the adsorption effect of the multi point surface of the graphene thin films. This gives the hybrid hydrogel more processing capacity due to its superimposed effect.

Next, we compared the adsorption photocatalytic properties of different composites (Fig. 9b) and found that when the content of  $\text{g-C}_3\text{N}_4$  nano-sheets increases, the catalytic capacity increases after adsorption equilibrium. This is because the bare rGH cannot undergo a photocatalytic reaction. The removal of Cr (VI) occurs

**Table 3**Adsorption kinetics parameters of rGH and 90% g-C<sub>3</sub>N<sub>4</sub>/rGH.

C <sub>0</sub>	q <sub>e,cal</sub> (mg/g)	Pseudo-first Kinetics		Pseudo-second Kinetics				
		k <sub>1</sub> (h <sup>-1</sup> )	q <sub>e,cal</sub> (mg/g)	R <sup>2</sup>	k <sub>2</sub> (g/mg h)	q <sub>e,cal</sub> (mg/g)	h (mg/g.h)	R <sup>2</sup>
30 mg/L rGH	16.75	0.03	9.47	0.844	7.7*10 <sup>-3</sup>	17.86	2.451	0.999
90% g-C <sub>3</sub> N <sub>4</sub> /rGH	23.74	0.03	6.11	0.844	2.1*10 <sup>-2</sup>	24.39	12.5	0.999

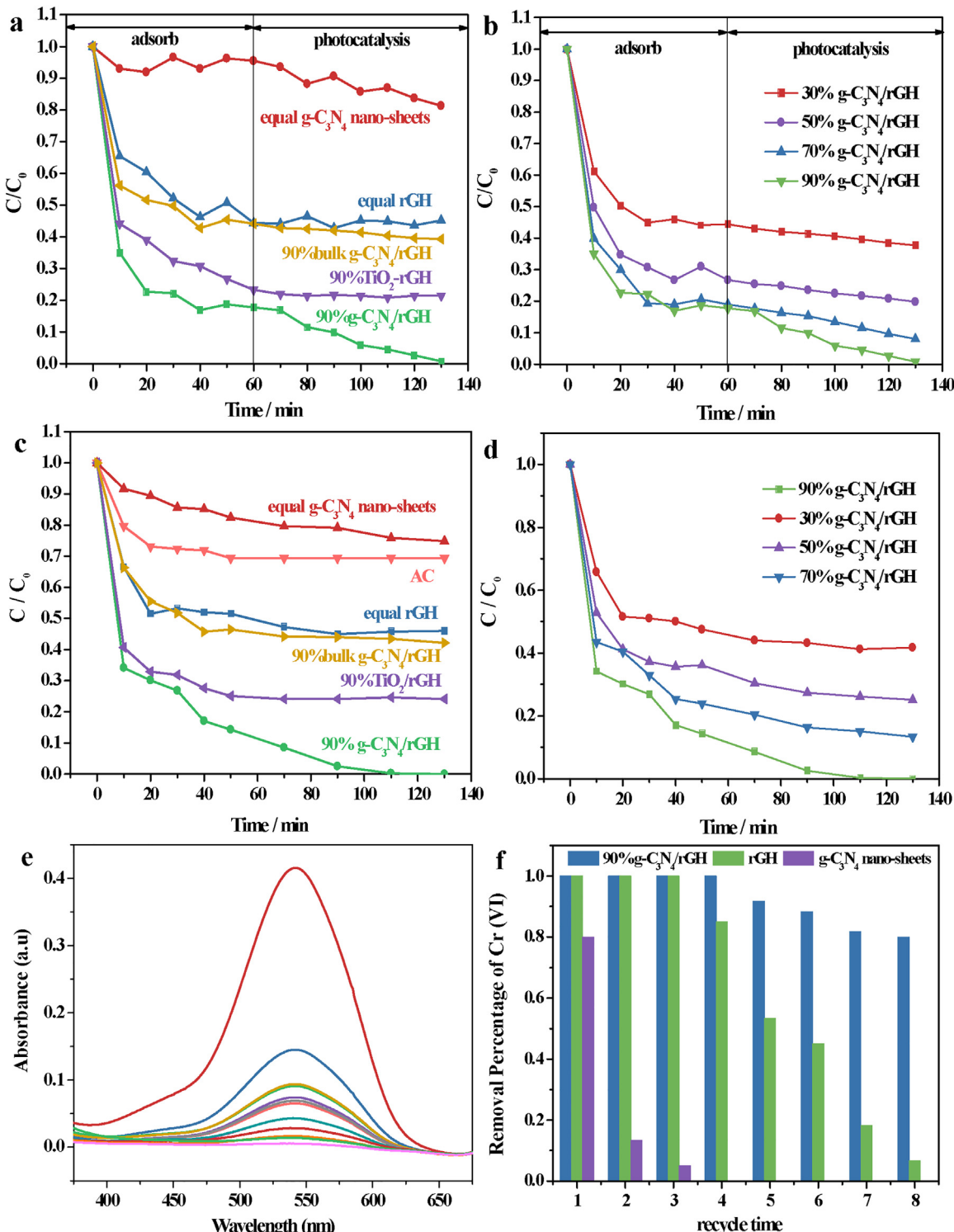


**Fig. 9.** (a) Adsorption and photo-catalysis capacity of different composite materials for removal of Cr(IV). (b) The adsorption and photo-catalysis capacity of a series of hybrid hydrogels for removal of Cr(IV). (c) Removal of Cr(IV) with different composite materials via the synergistic effect of adsorption and photo-catalysis. (d) Removal of Cr(IV) with different composite materials by the adsorption and photo-catalysis. (e) UV-vis spectra of 90%  $\text{g-C}_3\text{N}_4/\text{rGH}$  removal Cr(IV). (f) Recycling runs of 90%  $\text{g-C}_3\text{N}_4/\text{rGH}$  in removing Cr(IV) without desorption.

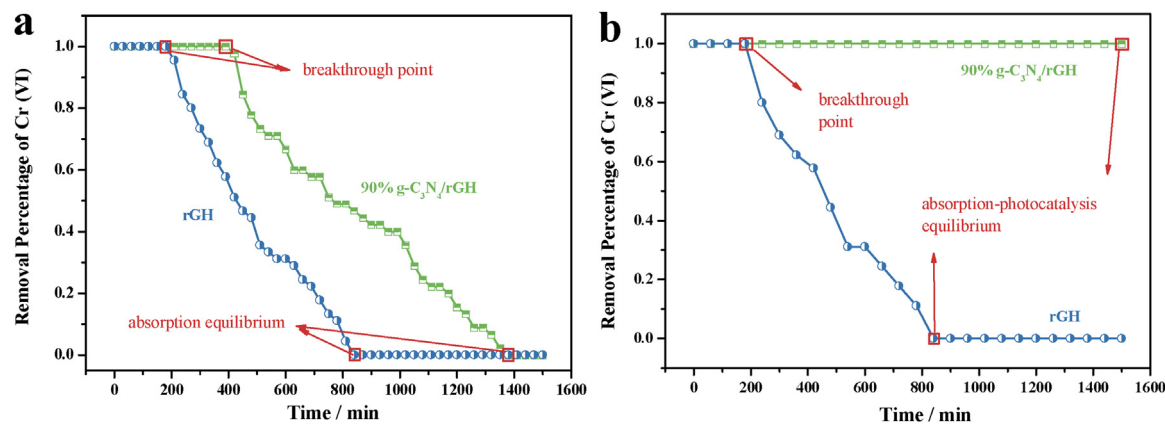


Fig. 10. Removal of Cr (VI) by 90% g-C<sub>3</sub>N<sub>4</sub>/rGH and rGH via continuous flow reaction: (a) in the dark and (b) under visible light.

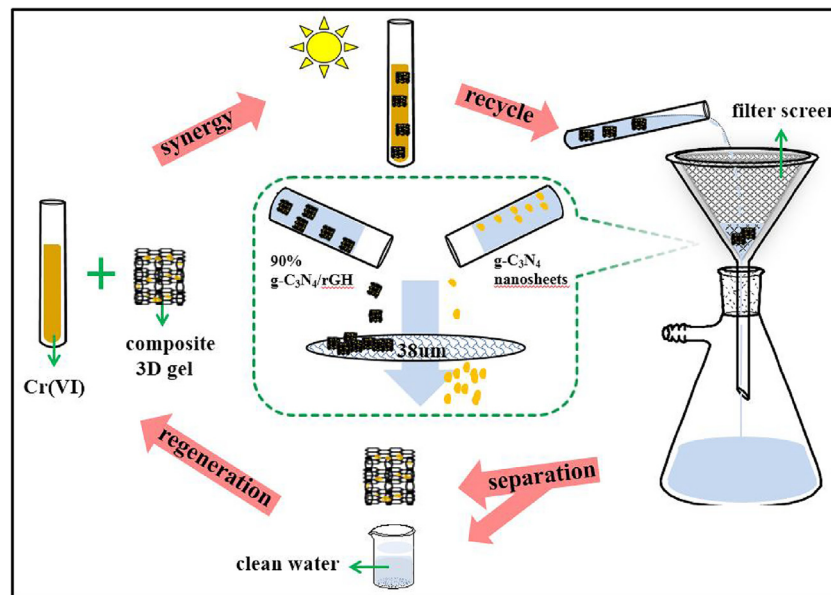


Fig. 11. Schematic of hybrid hydrogels processing.

via different composite materials under visible light (Fig. 9c). The synergistic effect of adsorption and photo-catalysis is obviously, because the adsorption capacity of the composites is larger than the photocatalytic ability. Thus, the degradation rate of the highest occurs within 10 min and then began to slow down. This is because g-C<sub>3</sub>N<sub>4</sub> nano-sheets and bulk g-C<sub>3</sub>N<sub>4</sub> have a visible light response. The related materials have a high degradation effect in which 90% g-C<sub>3</sub>N<sub>4</sub>/rGH has rich active sites and surface-adsorption in the degradation process. It can adsorb, assemble, and reduce the Cr (VI) *in situ*.

The rate of treatment was 3.98- and 1.85-fold that of g-C<sub>3</sub>N<sub>4</sub> nano-sheets and rGH, respectively. All composites in Fig. 9d show increased activity. The adsorption and photocatalytic activity of A is the best. The results show that the degradation rate of the complex is related to the content of g-C<sub>3</sub>N<sub>4</sub> nano-sheets, and the degradation rate increased with increasing content. This is shown in Fig. 9e there were no other by-products. The stability of the materials was tested (Fig. 9f), and nano size g-C<sub>3</sub>N<sub>4</sub> is difficult to recycle. This makes waste of resources difficult to recycle with a low rate of recycling. After three cycles of rGH, the adsorption reached saturation, and the treatment effect decreased sharply. The above results show that 90% g-C<sub>3</sub>N<sub>4</sub>/rGH overcomes the difficult recovery and adsorption saturation. The synergistic effect of adsorption and the

photo-catalysis effect can be effective in the treatment of low concentration Cr (VI) for a long time.

#### 3.4. Removal of Cr (VI) continuously and effectively in continuous flow reaction

The Cr (VI) was removed by 90% g-C<sub>3</sub>N<sub>4</sub>/rGH and rGH via a continuous flow reaction (Fig. 10). The general definition of the breakthrough point is the concentration of the outflow liquid is 3%~5% [44]. In this paper, the breakthrough point is the concentration when the outflow liquid is 5%. Removal of Cr (VI) in the dark is shown in Fig. 10a. The time needed for 90% g-C<sub>3</sub>N<sub>4</sub>/rGH (420 min) to reach the breakthrough point is more than rGH (210 min), and the time required for 90% g-C<sub>3</sub>N<sub>4</sub>/rGH (1380 min) to reach the saturation is more than rGH (810 min). This proved that the adsorption efficiency and adsorption capacity of composites were greatly improved.

Fig. 10b shows that the removal of Cr (VI) under visible light via the synergistic effect of adsorption and photo-catalysis. The rate of treatment of rGH is the same as in the dark, because of rGH has no visible light response. The breakthrough point of 90% g-C<sub>3</sub>N<sub>4</sub>/rGH disappeared, and heavy metal Cr (VI) remained completely degraded at 1500 min. The 90% g-C<sub>3</sub>N<sub>4</sub>/rGH for removal of

Cr (VI) (5 mg/L) in the cyclic tests maintained a high removal rate. This indicates that the g-C<sub>3</sub>N<sub>4</sub> nano-sheets combined with rGH for *in situ* adsorption and enrichment followed by catalytic and reduction into heavy metal Cr (VI). The synergistic effect of adsorption and photo-catalysis can be a long-term and effective treatment for low concentrations of Cr (VI).

### 3.5. Cycle and regeneration processing of hybrid hydrogels

In this experiment, we used a low cost and simple recovery method to recycle materials. This simulation of cyclic regeneration process is shown in Fig. 11. The hybrid hydrogel can rapidly degrade Cr (VI) from solution under visible light. It uses a stainless-steel filter to separate hydrogels under an atmospheric pressure. The hydrogel materials and purified water can then be separated quickly. The recycled of materials are not needed for further processing. This can be added to fresh polluted liquid, and the recycling process was realized. However, the g-C<sub>3</sub>N<sub>4</sub> nano-sheets cannot use the filter for effective separation before the composite g-C<sub>3</sub>N<sub>4</sub> nano-sheets and graphene hydrogel are formed. Therefore, the results show the advantage of the 3D network structure in the recovery and regeneration of the hydrogel materials.

## 4. Conclusions

In summary, we synthesized a free-metal g-C<sub>3</sub>N<sub>4</sub>/rGH hybrid hydrogel material that has a good response under visible light with easy recovery. This can improve the ability to treat Cr (VI) in water. The composites retain the rich active sites of g-C<sub>3</sub>N<sub>4</sub> nano-sheets and solve the problems of low agglomeration, low adsorption capacity, and difficult recovery of powder material. The high dispersion of the nano-sheets effectively increases the specific surface areas of the graphene hydrogel. This maintains the surface-adsorption characteristics of the 2D nano-sheets and improves the adsorption properties of the materials. The 3D hydrogel has significant synergistic effect of adsorption and photo-catalysis, when using 90% g-C<sub>3</sub>N<sub>4</sub>/rGH for adsorption and enrichment for *in situ* reduction of Cr (VI). The 30 mg/L Cr (VI) could be removed in 120 min, and the removal rate could still be maintained above 80% after 8 cycles (5 mg/L). The rate of recovery was up to 95%. In a continuous flow reaction, it realized a full and effective treatment at low concentrations (2 mg/L) of Cr (VI) within 1500 min. This attained the WHO's drinking water regulations as well as the EPA water Cr (VI) recommended concentration. This work further expands the application of photo-catalysis technology for heavy metal waste water treatment including downstream of industries.

## Acknowledgements

This work was financially supported by the National Natural Science Foundation of China (No. 51672081), Key Program of Natural Science of Hebei Province (B2016209375), Hebei Natural Science Funds for the Joint Research of Iron and Steel(B2016209348), Hebei Provincial Foundation for International cooperation(15391403D).

## References

- [1] B. Kiran, N. Rani, A. Kaushik, *J. Environ. Chem. Eng.* 4 (2016) 4137–4142.
- [2] C.M. Thompson, A. Bichteler, J.E. Rager, M. Suh, D.M. Proctor, L.C. Haws, M.A. Harris, *Mutat. Res. Genet. Toxicol. Environ. Mutagen.* 800 (2016) 28–34.
- [3] L.H. Wang, C.I. Lin, *J. Chin. Inst. Chem. Eng.* 39 (2008) 367–373.
- [4] A. Verma, R. Dua, A. Singh, N.R. Bishnoi, *Water sci.* 29 (2015) 19–25.
- [5] C.G. Lee, S. Lee, J.A. Park, C. Park, S.J. Lee, S.B. Kim, B. An, S.T. Yun, S.H. Lee, J.W. Choi, *Chemosphere* 166 (2017) 203–211.
- [6] A. Jain, R. Balasubramanian, M.P. Srinivasan, *Chem. Eng. J.* 283 (2016) 789–805.
- [7] M.A. Khan, B.H. Hameed, J. Lawler, M. Kumar, B.H. Jeon, *Desalin. Water Treat.* 54 (2015) 422–449.
- [8] V.K. Gupta, A. Nayak, B. Bhushan, S. Agarwal, *Crit. Rev. Env. Sci. Tec.* 45 (2015) 613–668.
- [9] W. Peng, H. Li, Y. Liu, S.X. Song, *J. Mol. Liq.* 230 (2017) 496–504.
- [10] A.S. Rad, *J. Alloys Compd.* 682 (2016) 345–351.
- [11] S.L. Wan, F. He, J.Y. Wu, W.B. Wan, Y.W. Gu, B. Gao, *J. Hazard. Mater.* 314 (2016) 32–40.
- [12] Y.Q. Chen, L.B. Chen, H. Bai, L. Li, *J. Mater. Chem. A* 1 (2013) 1992–2001.
- [13] A.V. Avdeenkov, I.V. Bodrenko, D.G. Bessarabov, A.V. Bibikov, A.V. Nikolaev, M.D. Taran, A. Tokarev, E.V. Tkalya, *Int. J. Hydrogen Energy* 40 (2015) 4184–4193.
- [14] Y.B. Cheng, P. Xu, W. Zeng, C.X. Ling, S. Zhao, K. Liao, Y.M. Sun, A.J. Zhou, *J. Environ. Chem. Eng.* 5 (2017) 1957–1963.
- [15] T. Fang, X.M. Yang, L.Z. Zhang, J.M. Gong, *J. Hazard. Mater.* 312 (2016) 106–113.
- [16] J. Liu, Y. Liu, N.Y. Liu, Y.Z. Han, X. Zhang, H. Huang, Y. Lifshitz, S.T. Lee, J. Zhong, Z.H. Kang, *Science* 347 (2015) 970–974.
- [17] L. Zhou, H.Y. Zhang, H.Q. Sun, S.M. Liu, M.O. Tade, S.B. Wang, W.Q. Jin, *Catal. Sci. Technol.* 6 (2016) 7002–7023.
- [18] X.J. Bai, L. Wang, R.L. Zong, Y.F. Zhu, *J. Phys. Chem. C* 117 (2013) 9952–9961.
- [19] G.H. Dong, L.Z. Zhang, *J. Phys. Chem. C* 117 (2013) 4062–4068.
- [20] M. Zhang, W.J. Luo, Z. Wei, W.J. Jiang, D. Liu, Y.F. Zhu, *Appl. Catal. B* 194 (2016) 105–110.
- [21] S. Samanta, S. Khilari, D. Pradhan, R. Srivastava, *ACS Sust. Chem. Eng.* 5 (2017) 2562–2577.
- [22] F.H. Liu, J. Yu, G.Y. Tu, L. Qu, J.C. Xiao, Y.D. Liu, L.Z. Wang, J.Y. Lei, J.L. Zhang, *Appl. Catal. B* 201 (2017) 1–11.
- [23] Z.X. Zhou, J.H. Wang, J.C. Yu, Y.F. Shen, Y. Li, A.R. Liu, S.Q. Liu, Y.J. Zhang, *J. Am. Chem. Soc.* 137 (2015) 2179–2182.
- [24] X.J. Bai, L. Wang, R.L. Zong, Y.F. Zhu, *J. Phys. Chem. C* 117 (2013) 9952–9961.
- [25] J.S. Zhang, M.W. Zhang, C. Yang, X.C. Wang, *Adv. Mater.* 26 (2014) 4121–4126.
- [26] Q.J. Xiang, J.G. Yu, M. Jaroniec, *Chem. Soc. Rev.* 41 (2012) 782–796.
- [27] J. Zhang, Z.P. Zhu, Y.P. Tang, K. Müllen, X.L. Feng, *Adv. Mater.* 26 (2014) 734–738.
- [28] P. Chen, X. Liu, R. Jin, W. Nie, Y. Zhou, *Carbohyd. Polym.* 167 (2017) 36–43.
- [29] R.K. Sharma, Y.N. Chouriyal, S. Chaudhari, J. Saravanan, S.R. Dey, P. Ghosh, *ACS Appl. Mater. Interfaces* 9 (2017) 11651–11661.
- [30] W.C. Wan, S. Yu, F. Dong, Y. Zhou, *J. Mater. Chem. A* 4 (2016) 7823–7829.
- [31] M. Zhang, W.J. Luo, Z. Wei, W.J. Jiang, D. Liu, Y.F. Zhu, *Appl. Catal. B* 194 (2016) 105–110.
- [32] Y. Li, W.Q. Cui, L. Liu, R.L. Zong, W.Q. Yao, Y.H. Liang, Y.F. Zhu, *Appl. Catal. B* 199 (2016) 412–423.
- [33] J. Xu, L. Wang, Y.F. Zhu, *Langmuir* 28 (2012) 8418–8425.
- [34] A. Singh, A. Sharma, M. Tomar, V. Gupta, *Sensor. Actuat. B-Chem.* 245 (2017) 590–598.
- [35] T.G. Xu, L.W. Zhang, H.Y. Cheng, Y.F. Zhu, *Appl. Catal. B* 101 (2011) 382–387.
- [36] W.J. Jiang, W.J. Luo, J. Wang, M. Zhang, Y.F. Zhu, *J. Photoch. Photobio. C Photoch. Rev.* 28 (2016) 87–115.
- [37] K.C. Kemp, H. Seema, M. Saleh, N.H. Le, K. Mahesh, V. Chandra, K.S. Kim, *Nanoscale* 5 (2013) 3149–3171.
- [38] S.C. Yan, Z.S. Li, Z.G. Zou, *Langmuir* 25 (2009) 10397–10401.
- [39] I.V. Lightcap, T.H. Kosel, P.V. Kamat, *Nano Lett.* 10 (2010) 577–583.
- [40] H.P. Cong, X.C. Ren, P. Wang, S.H. Yu, *ACS Nano* 6 (2012) 2693–2703.
- [41] K. Dai, L.H. Lu, Q. Liu, G.P. Zhu, X.Q. Wei, J. Bai, L.L. Xuan, H. Wang, *Dalton Trans.* 43 (2014) 6295–6299.
- [42] S.W. Hu, L.W. Yang, Y. Tian, X.L. Wei, J.W. Ding, J.X. Zhong, P.K. Chu, *Appl. Catal. B* 163 (2015) 611–622.
- [43] W.J. Fang, J.Y. Liu, L. Yu, Z. Jiang, W.F. Shangguan, *Appl. Catal. B* 209 (2017) 631–636.
- [44] E. Malkoc, Y. Nuhoglu, Y. Abali, *Chem. Eng. J.* 119 (2006) 61–68.